Structural and Multidisciplinary Optimization (2022) 65:213
https://doi.org/10.1007/s00158-022-03322-w

RESEARCH PAPER

A machine learning accelerated inverse design of underwater acoustic polyurethane coatings

Hansani Weeratunge[1] · Zakiya Shireen[1] · Sagar Iyer[1] · Adrian Menzel[2] · Andrew W. Phillips[2] · Saman Halgamuge[1] · Richard Sandberg[1] · Elnaz Hajizadeh[1]

Received: 13 April 2022 / Revised: 31 May 2022 / Accepted: 23 June 2022 / Published online: 5 August 2022

Abstract
Here we propose a detailed protocol to enable an accelerated inverse design of acoustic coatings for underwater sound attenuation application by coupling Machine Learning and an optimization algorithm with Finite Element Models (FEM). The FEMs were developed to obtain the realistic performance of the polyurethane (PU) acoustic coatings with embedded cylindrical voids. The frequency dependent viscoelasticity of PU matrix is considered in FEM models to substantiate the impact on absorption peak associated with the embedded cylinders at low frequencies. This has been often ignored in previous studies of underwater acoustic coatings, where usually a constant frequency-independent complex modulus was used for the polymer matrix. The key highlight of the proposed optimization framework for the inverse design lies in its potential to tackle the computational hurdles of the FEM when calculating the true objective function. This is done by replacing the FEM with an efficiently computable surrogate model developed through a Deep Neural Network. This enhances the speed of predicting the absorption coefficient by a factor of 4.5×10^3 compared to FEM model and is capable of rapidly providing a well-performing, sub-optimal solution in an efficient way. A significant, broadband, low-frequency attenuation is achieved by optimally configuring the layers of cylindrical voids. This is accomplished by accommodating attenuation mechanisms, including Fabry–Pérot resonance and Bragg scattering of the layers of voids. Furthermore, the proposed protocol enables the inverse and targeted design of underwater acoustic coatings through accelerating the exploration of the vast design space compared to time-consuming and resource-intensive conventional trial-and-error forward approaches.

Keywords Deep Neural Network · Optimization · Metamaterials · Polyurethane elastomers · Underwater acoustic coatings

1 Introduction

Acoustic coating technologies (Fu et al. 2021) have been installed on maritime platforms for a variety of sound attenuation purposes since the twentieth century and have been continuously improved to address evolving performance requirements (Meyer et al. 1958). However, with the advent of advanced sonar technologies, achieving an effective sound attenuation in the low frequency range has been a formidable challenge due to the corresponding long wavelengths, as it involves impractically thick coating requirements and/or increase in embedded cavity diameters. In addition, underwater vessels with thick coatings lead to a compromised resistant to hydrostatic pressure.

Elastomers have proven to be the material of choice for anechoic coatings due to their underlying microstructure, viscoelasticity, and inherent relaxation mechanisms (Jayakumari et al. 2019).

Furthermore, the combinatorial structure of soft elastomeric coating layer with embedded voids or rigid inclusions of different shapes results in the appearance of resonance phenomenon, which leads to the desired reduction in sound transmission at low-frequency band (Liu et al. 2000; Fu et al. 2021; Wen et al. 2011; Sharma et al. 2019; Calvo et al. 2015). The low frequency sound attenuation has also been achieved by multi-layered composite materials with different

Responsible Editor: Lei Wang

✉ Elnaz Hajizadeh
ellie.hajizadeh@unimelb.edu.au

[1] Department of Mechanical Engineering, Faculty of Engineering and Information Technology, The University of Melbourne, Parkville, Australia

[2] Maritime Division, Defence Science and Technology Group, Melbourne, Australia

natural resonant frequencies in each layer (Shi et al. 2019), and by creating periodically distributed voids in the viscoelastic matrix (Alberich-type coatings) Ivansson (2008).

Topological optimization is one of the key techniques to design anechoic coatings with embedded inclusions, which determines the optimal size and layout of inclusions within the polymer matrix instead of a specific configuration. This leads to an enhanced sound attenuation due to the increased degrees of freedom (Li and Li 2018; Gao et al. 2019; Yu et al. 2020).

Design of acoustic coatings has been conventionally done through employing a *forward approach*, which involves an iterative evaluation of developed designs to predict the acoustic performance by computational or experimental means. For high dimensional design space, forward approach becomes computationally expensive and time-intensive. Nevertheless, the fundamental problem in material design for a specific performance demands an inverse approach, i.e., finding the corresponding design parameters which deliver a *targeted performance*. In the inverse design approach, one can utilize the forward predictive models to compare the performance of the designed materials with the target performance (ground truth). Thus, the inverse design process can be formulated as an optimization problem that minimizes the difference between the models developed through the forward approach and the ground truth (Zhong et al. 2019). Traditionally, this gap is minimized using empirical trial-and-error methods in conjunction with prior domain knowledge. With technological advancements and increased computational power, efficient optimization algorithms and data-driven techniques, such as machine learning (ML) are employed to automate the learning process while utilizing physics-based understanding (Bacigalupo et al. 2020; Donda et al. 2021; Ahmed et al. 2021; Sun et al. 2021; Gurbuz et al. 2021; Zheng et al. 2020; Wu et al. 2021; Bianco et al. 2019; Wu et al. 2022) through physical models.

In the forward approach, analytical and numerical models have been developed to evaluate the acoustic performance of inclusions in a variety of mediums. However, analytical models are usually limited to simple cases, including assumptions with respect to the viscoelastic nature of the polymer matrix and distribution of the inclusions (Cai et al. 2006; Leroy et al. 2015). Alternatively, numerical models such as finite element model (FEM) (Cai et al. 2006; Panigrahi et al. 2008) and layer multiple scattering theory (Yuan et al. 2019) are commonly used to predict the acoustic performance of these coatings (Meng et al. 2012a). However, most of these studies overlook the crucial frequency dependent viscoelastic properties of the polymer matrix, although it significantly alters the acoustic characteristics of the coating.

To reverse engineer acoustic coatings with embedded voids to achieve desired acoustic performance, metaheuristic optimization techniques such as genetic algorithms (GA) (Meng et al. 2012a; Yuan et al. 2019; Chang et al. 2005; Wang et al. 2021) and evolutionary algorithms (EA) (Romero-García et al. 2009; Zhao et al. 2018) are widely used. Interest has been given to GA as it can be used to find a near-optimal solution efficiently (Meng et al. 2012a; Yuan et al. 2019; Chang et al. 2005). These techniques can provide a well performing and efficient sub-optimal solution to non-linear, non-convex optimization problems. However, these classical iterative optimization algorithms tend to become highly time consuming and computationally demanding due to the iterative evaluation of the objective function. Furthermore, the computational efforts could grow exponentially with increasing dimension of the design space, i.e., the number of optimization variables (Wu et al. 2021). Therefore, systematic, and efficient computational models are key in implementing and speeding up of the optimization algorithms.

In recent years, the application of Deep Neural Networks (DNNs) has become a promising tool due to their ability to capture nonlinear dynamics in complex models. The use of DNNs have been reported for accelerated and accurate prediction of the acoustic performance of materials (Ciaburro et al. 2021; Jeon et al. 2020; Iannace et al. 2020; Ciaburro et al. 2020). Although these models have achieved considerable success in recent years, they still suffer from issues of interpretability, i.e., lack of understanding of the rationale behind the predictions (Angione et al. 2022). However, techniques of interpretation such as sensitivity analysis may be used to explore and extract new insights from the complex physical system (Montavon et al. 2018).

1.1 Contribution and Focus

In the present work, we have developed a framework for accelerated and targeted design of underwater acoustic coatings with embedded resonant inclusions through combining FEM models with ML and optimization algorithms. This framework enables (1) fast exploration of the design space and (2) an inverse targeted design strategy compared to the conventional forward trial-and-error coating design approaches. The coatings (anechoic tiles) are composite materials based on elastomeric polyurethane matrices with cylindrical resonant inclusions as they couple strongly with water-borne acoustic waves (Leroy et al. 2015). Additionally, contrary to other shapes of voids, cylindrical voids resonate at desired lower frequencies (Ivansson 2012; Sharma et al. 2017a).

The developed framework focuses on inverse design of acoustic coatings with only two layers of cylindrical voids to accommodate for the constraints on the maximum allowable thickness of the tiles as well as desired large cylinders. We focus on optimizing the geometric design parameters (as shown in Fig. 1c) of the PU matrix

with embedded cylindrical voids. The optimal size and layout of layers of cylindrical voids are key determining factors to achieve a significant broadband attenuation in the low frequency range. The ML-based inverse design addresses and resolves the computational limitations of the time intensive FEM for calculating the true objective function. In our framework, we replace the FEM with an efficient ML based surrogate model developed through DNN. The developed framework performs expeditiously and provides a sub-optimal solution which consequently results in higher absorption. Using the ML model, we have demonstrated the enhancement of the speed of prediction by a factor of 4.5×10^3. In addition, in our FEM, we have accounted for the crucial frequency and temperature dependent complex moduli of the polyurethane (PU) elastomers, which have been ignored in previous studies of similar systems (Sharma et al. 2019). To achieve this, the complex moduli data obtained from experimental Dynamic Mechanical Analysis (DMA) is incorporated into the FEM model.

The outline of the study and forward and inverse components of the optimization framework shown in Fig. 1a are as follows:

- We solve the forward problem by linking the material and geometrical parameters of the polyurethanes and cylindrical voids to their acoustic behavior through a FEM, where we also account for the temperature and frequency dependence of the Young's and shear moduli of the matrix polyurethanes.
- The Young's and shear moduli master curves are obtained by employing the time–temperature superposition (TTS) principle on experimental data obtained from DMA measurements.
- Data from the FEM is used to develop a deep neural network that accurately predicts the absorption coefficient of the composites for different design parameters.
- In the inverse targeted design component, the neural network model is integrated with genetic algorithm to determine the optimal geometrical parameters for each polyurethane matrix composite to maximize broad-band sound absorption at low frequencies.

The manuscript is organized as follows. Section 2 describes the models developed to establish the optimization framework. Section 2 includes FEM description (Sect. 2.1), inverse design using optimization approach (Sect. 2.2),

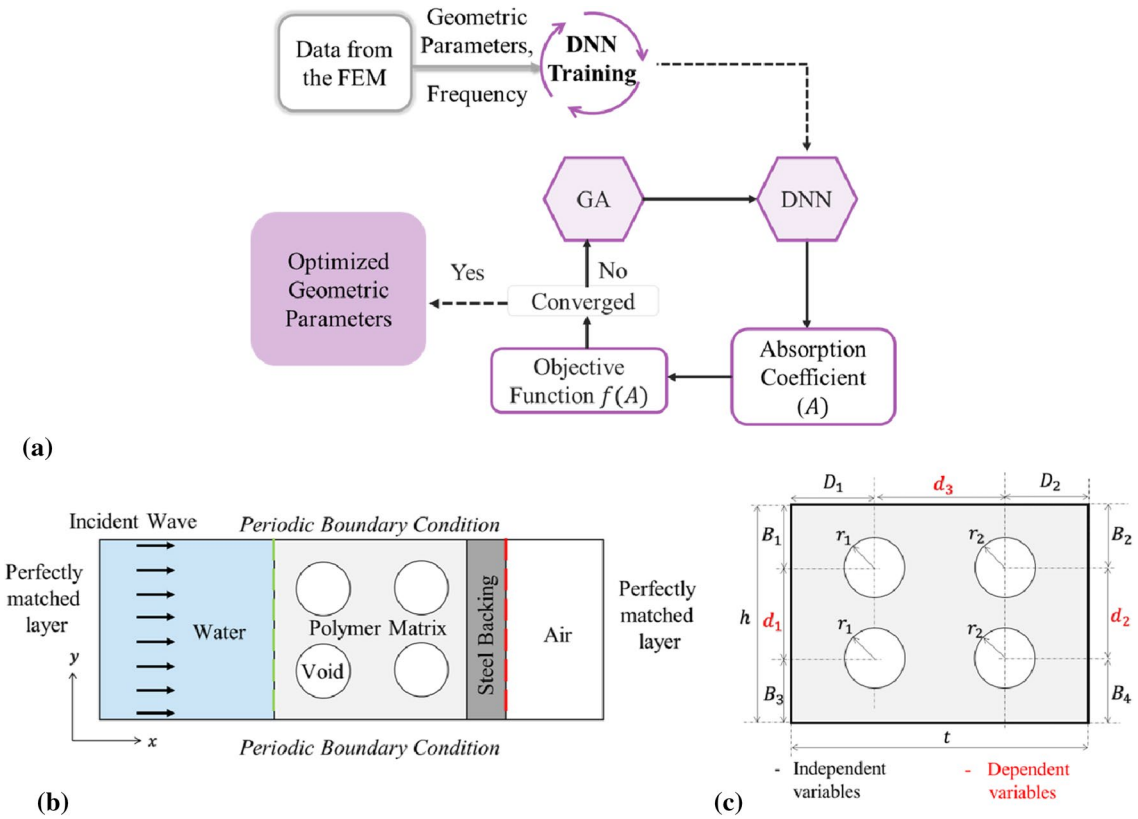

Fig. 1 **a** The schematic representation of the proposed optimization framework. **b** 2D schematic diagram of the unit cell of model polymer matrix composite with four cylindrical voids. **c** Schematic representation of the design space including the geometrical variables for the 2D COMSOL model

followed by accelerated forward approach using deep neural network (Sect. 2.3). In Sect. 3, the findings of the work are reported in multiple subsections. Section 3.1 describes the parametric study of the FEM, which includes the effect of frequency-dependent moduli of the PU matrix (Sect. 3.1.1). Extension of this parametric study that explores the effect of voids (Section 3.1), the effect of polyurethane matrix (Section 3.2), and finally effect of steel backing (Section 3.3) on sound attenuation is presented in the supplementary information. In Sect. 3.2, the performances of optimized acoustic coatings with voids in three different polyurethanes (PU80 (Sect. 3.2.1), PU65 (Sect. 3.2.2) and PU90 (Sect. 3.2.3)) are compared and discussed in detail. Finally, Sect. 4 summarizes the conclusions emphasizing the potential of ML approaches in numerical modeling and how the results from this work can be used in further research.

2 Methods and Models

In acoustic coatings with embedded voids, peak values of the sound absorption coefficient usually correspond to the resonance frequency of the voids. However, the bandgap of this peak may be narrow as it only occurs around the resonance frequency. Therefore, adding multiple voids of different sizes can broaden the bandgap as each of the voids resonates at their natural frequency and results in multiple absorption peaks (Fu et al. 2021). In this study, four cylindrical voids in two different layers with different radii in each layer with varied spacing have been considered per unit cell. This creates more possibilities for maximizing the absorption coefficient in a wider range of frequencies.

2.1 Finite element model (FEM)

A 2-dimensional FEM was developed using acoustic and solid mechanics modules of the COMSOL Multiphysics Software Package version 5.5 to explore the underwater acoustic behavior of a slab of PU matrix with cylindrical voids. We have incorporated frequency-dependent dynamic moduli of the polymer matrix obtained from a DMA (master curves obtained from DMA data are given in Fig. S1a in the supplementary information). This allows the development of accurate models, which account for the realistic viscoelastic behavior of the polymer matrix and its potential impact on the overall performance of the acoustic coating.

We considered the cross-section of two layers of cylindrical voids in a PU matrix attached to a steel backing submerged in water as schematically depicted in Fig. 1b. Periodic boundary conditions were applied to an infinite array of units in the y direction. The acoustic plane wave was propagated in the x direction and is perpendicular to the y axis. Furthermore, perfectly matching layers were applied at the end of the water layer and air layer to mimic an open and non-reflecting infinite domain. The transmitted pressure was measured at the steel-air interface (the dashed red line), and the reflection was measured at the water-polymer interface (dashed green line). The polymer domain and steel were modeled as viscoelastic solid and elastic solid materials, respectively. The densities of PU and steel were taken as 1026 kg m^{-3} and 7850 kg m^{-3}, respectively at temperature $T = 15$ °C and pressure $P = 101.325$ kPa. The thickness of the steel backing was considered 30 mm. For air and water, the inbuilt material properties available in the COMSOL materials library were used. The developed FEM models have been validated against data from literature (Jayakumari et al. 2011; Sharma et al. 2017b), and it is presented in Section 2 in the supplementary information.

2.2 Inverse design approach using optimization

One of the common and longstanding issues in designing anechoic coatings with embedded voids is the relatively narrow absorption peak produced by the voids (Jayakumari et al. 2019). In the present study, we develop an inverse design and optimization framework shown in Fig. 1a to maximize the low-frequency sound attenuation while increasing the bandwidth of the peak. In Fig. 1b, the schematic of the unit cell of PU matrix composite is shown with four cylindrical voids and is considered for optimization. An array of $2 \cdot 2$ voids in the unit cell was considered to account for all the influencing geometrical parameters. This ensures the possibility of exploring a wider design space to find a better solution for a maximized low-frequency broad-band sound attenuation. Furthermore, the design variables of the model are shown in Fig. 1c.

The developed optimization scheme was formulated using the GA as it is an evolutionary-based meta-heuristic search algorithm that mimics the natural selection of a population with the process of adaptation for survival. Genetic algorithm is considered a robust and efficient approach that can be used to explore complex nonlinear solution spaces (Katoch et al. 2021). Unlike swarm intelligence techniques, GA is less likely to have a premature convergence to a local optimal solution (Katoch et al. 2021). For the optimization algorithm in this study, 10 independent geometrical parameters of the unit cell (shown in Fig. 1c) were considered as the design variables for which objective function is defined as Eq. 1,

$$\text{Objective function} = \max\left(\sum_{i=1}^{N} w_i a_i - p\right), \quad w_i = \frac{N+1-i}{N}, \tag{1}$$

where w_i and a_i are the weight and absorption coefficient of the ith frequency, respectively and N is the number of frequencies. 1000 frequency points were considered ranging from 10 Hz to 10 kHz with equal intervals of 10 Hz. In the objective function, the weighted sum of the absorption coefficient was considered for the whole frequency range but higher weights have been allocated to low frequencies to provide a higher priority to the low frequency range attenuation. Furthermore, a penalty p was included in the objective function to add manufacturing, or practical constraints to avoid infeasible solutions. A constraint was employed to maintain a minimum distance of 1 cm between the edges of the coating and the voids considering the practical fabrication processes. Larger values of penalty were imposed for solutions that violate the constraints. Additionally, the feasible limits of the design variables were directly incorporated into the GA by setting reasonable lower and upper bounds for the variables presented in Table 1.

The transmission coefficient of the acoustic coatings with embedded voids is negligible due to the large impedance mismatch between the steel plate and the air backing (a detailed explanation is given in supplementary information S3.3). Therefore, a maximized absorption coefficient is equivalent to a minimized reflection coefficient given their relationship through the following equations

$$\begin{aligned} A + T + R &= 1, \\ T &\approx 0, \\ A + R &= 1 \end{aligned} \tag{2}$$

where A, T and R are absorption, transmission and reflection coefficients, respectively. Hence, the optimized design of the proposed algorithm will exhibit better anechoic properties with a low reflection coefficient.

Table 1 Lower and upper bounds of the design variables

Design variable	Lower bound/(mm)	Upper bound/(mm)
r_1, r_2	1	15
D_1, D_2	10	80
B_1, B_2, B_3, B_4	10	80
h	30	100
t	30	100

2.3 Accelerated forward approach using Deep Neural Network (DNN)

In optimization algorithms, the high computational cost of high fidelity physical models such as FEM becomes an obstacle in practical implementation. Therefore, approximations or surrogate models with less computational costs can be constructed to replace the high fidelity model. Conventionally, surrogate models were constructed based on statistical methods through linear, polynomial regression, or a combination of basis functions (Wu et al. 2021). However, with the recent advances in machine learning, the application of artificial neural networks (ANN) is widespread due to their ability to capture nonlinear dynamics in complex models. Artificial neural network is a ML technique that mimics the process of the nervous system in the brain. It is used as a basis to develop algorithms with the ability to learn, identify complex patterns, and extract key features from data sets. DNNs are one of the widely used supervised learning models used to develop predictive models in numerous applications.

DNN can transform a set of input variables into corresponding outputs by approximating the existing nonlinear relationship. The DNN learns this approximation by 'training', i.e., the iterative adjustment of its network parameters to capture the implicit mapping of the input and output variables. This is achieved by utilizing an optimization algorithm to minimize the error between the predicted and actual output. A well-structured and well-trained neural network can accurately predict the output corresponding to a set of previously unseen inputs.

To predict the absorption coefficient of the model shown in Fig. 1b, a DNN with multiple hidden layers is developed in Python using Scikit-learn (Note, three separate DNNs were developed to predict the absorption coefficient of the three commercial polyurethanes considered in this study). This DNN is used as a surrogate model to accelerate the forward prediction of the acoustic behavior of the coatings with embedded cylindrical voids.

The trained DNN is integrated into the optimization algorithm to expedite the exploration of the best set of parameters that yields low frequency broadband sound attenuation. We employed a multi-layer feed forward neural network with multiple hidden layers as shown in Fig. 2a to predict the absorption coefficient of the acoustic coatings with embedded voids. The input layer considers ten independent geometrical parameters (shown in Fig. 1c) as well as the frequency as inputs. For the enhanced performance of the network, the inputs were converted to a common scale by normalizing to a value between (0, 1).

The accuracy of the network was evaluated using the mean absolute percentage error (MAPE) that calculates the deviation between the predicted and actual values.

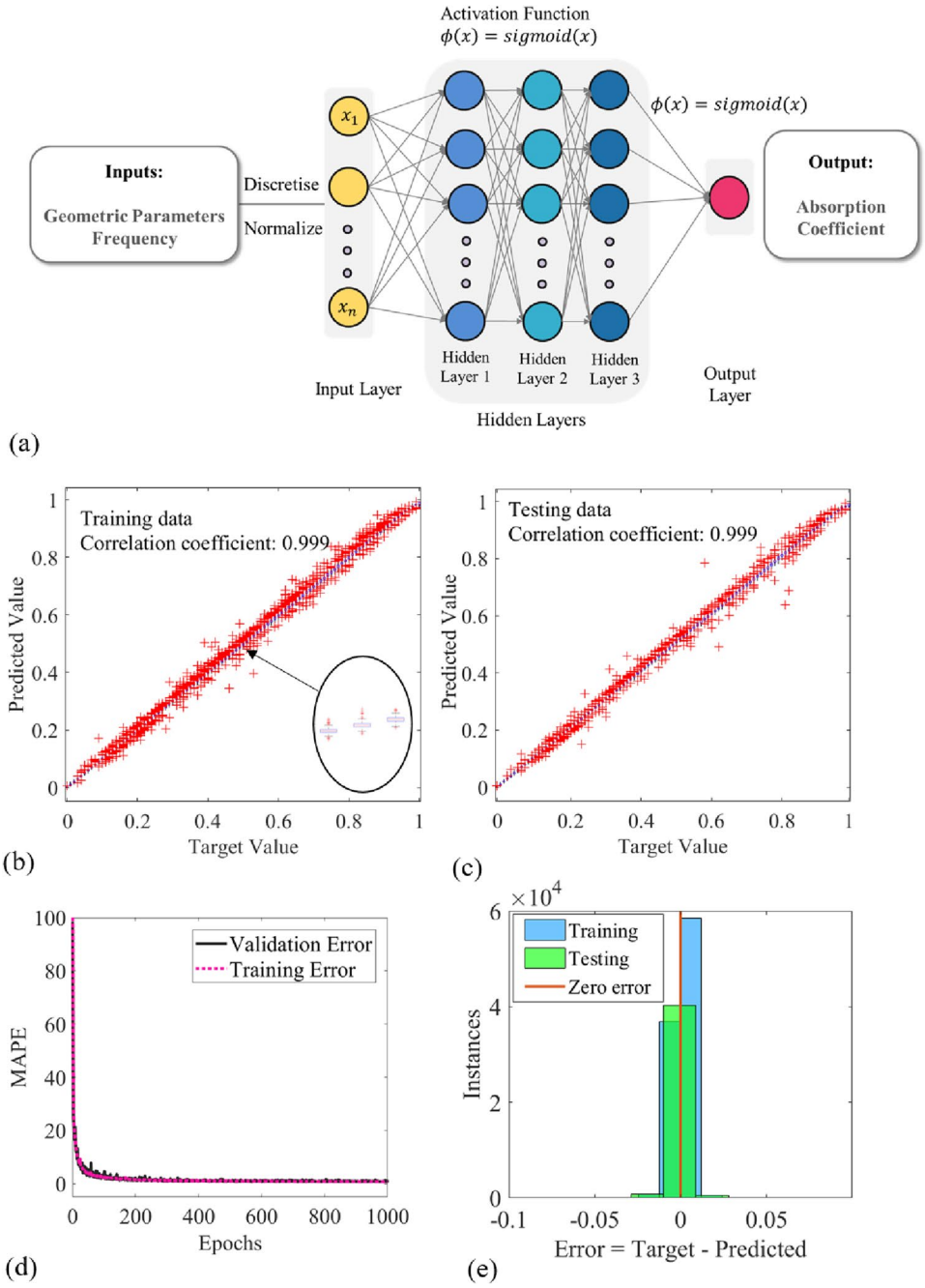

Fig. 2 **a** The general architecture of the DNN developed to predict the absorption coefficient. **b** Variation of the predicted (by DNN) and targeted (calculated from the Comsol FEM model) absorption coefficient for the training data. **c** Variation of the predicted and targeted absorption coefficient for the testing data. **d** Performance analysis of the neural network during training. **e** Error histogram of the neural network

Multiple DNN architectures with different activation functions, learning rate, number of layers and nodes were evaluated, and the best architecture was then selected based on the lowest MAPE and the least overfitting. Accordingly, sigmoidal activation functions were used in the network's intermediate layers to activate the signals in the nodes due to their enhanced performance compared to other activation functions. The sigmoid function returns values between (0 and 1) that align with the range of the data in this study. The network is optimized using the Adam optimizer, which is a stochastic gradient descent algorithm based on adaptive estimates of lower-order moments (Kingma and Ba 2015).

2.3.1 DNN performance for coating with voids in PU80

For training the DNN, we collected approximately 150, 000 data points from the COMSOL FEM models. This encompasses 400 sets of combinations of geometric parameters achieved through randomization within the desired range (presented in Table 1). The simulations were carried out in the low frequency range, i.e., 10 Hz–10

kHz. The data were randomly split into two sets. 70% of the data were randomly selected to train the model and the remaining 30% of the data are considered for testing. Furthermore, 20% of the training data were randomly selected for validation. The generality of the network and its performance were evaluated for unseen data. Accurate predictions were achieved with just three hidden layers that contain 200 nodes (neurons) at each layer. The optimized learning rate, batch size and the number of epochs was 0.0021, 100, and 800, respectively. The convergence of the network during the training process is presented in Fig. 2d. Further, the computation time to converge the network from a 2.3 GHz core i7 processor is approximately 820s.

The performance of the trained neural network was investigated by comparing the target value and the predicted value for the absorption coefficient. Figure 2b and c present the distributions of the predictions and the line of equality (identity line) for the training and testing data where the x and y axes are the targets and the predicted values, respectively. The central mark on each blue box represents the median, and the upper and lower edges indicate 25th and 75th quartiles. The outliers are plotted individually in red '+' symbols. The scatter points are closer to the line of equality, which indicates the reliability and accuracy of the prediction. The developed DNN showed a Pearson coefficient (R) of 0.999 for predicted test data and MAPE of 1.22, 1.27, and 1.27 for the training, validation, and testing data, respectively. Furthermore, as seen in the error histogram in Fig. 2e, the majority of the predictions are closer to zero error. Therefore, the predicted absorption coefficient from the DNN is in good agreement with the FEM model. The average prediction time for a frequency range from 10 Hz to 10 kHz in steps of 20 Hz for the DNN is approximately 0.04 s, whereas the FEM takes an average of 180 s. This pinpoints the speed increase by a factor of 4.5×10^3 compared to FEM, and therefore, significantly accelerates the optimization process.

3 Results and Discussion

3.1 Parametric study of finite element model

We have investigated the impact and physical mechanisms of varying material properties of the polymer matrix as well as geometrical parameters of the cylindrical voids. We also explored the effect of the layout of the cylindrical voids on the acoustic performance of the PU80 matrix composite. The detailed discussion is presented in the supplementary information Sections 3.1–3.3.

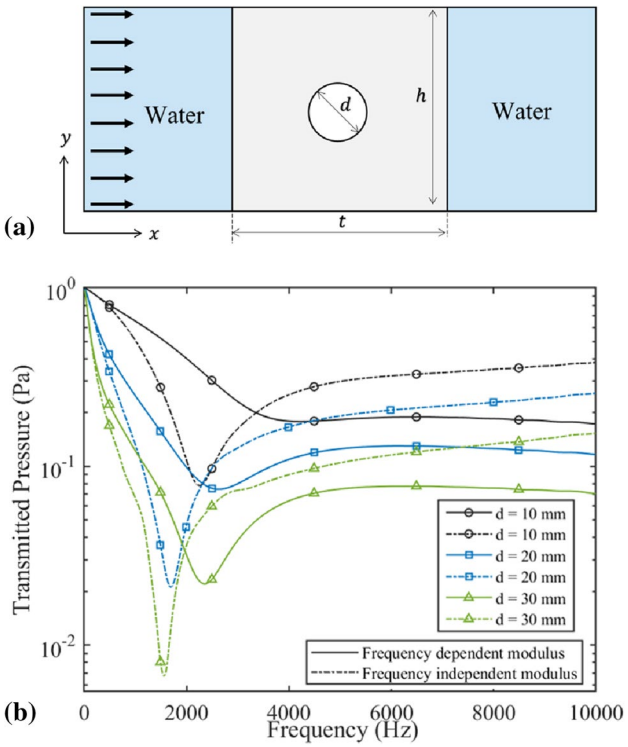

Fig. 3 **a** A schematic representation of a model with a single layer of cylindrical voids in PU matrix submerged in water. **b** Transmitted acoustic pressure through PU80 matrix for a range of void diameters. Solid lines represent the frequency-dependent modulus and dashed lines represent the frequency independent modulus

3.1.1 Frequency dependent PU moduli

In order to consider realistic material properties, frequency-dependent Young's modulus for PU80 (as shown in Fig. S1a) was considered. Frequency dependence of sound attenuation of a single layer of voids embedded in the PU matrix (shown in Fig. 3a) was evaluated by considering frequency-independent complex Young's modulus at 100 Hz ($8.8 + 2.3i$ MPa). The sound attenuation by voids is attributed to their monopole resonance, which results in a reduction in the transmitted acoustic pressure at their resonance frequency (Sharma et al. 2017a). The attenuation is also affected by the void diameter d, thus, we varied the void size while keeping the thickness $t = 10$ cm and the spacing between the voids, i.e., the lattice constant $h = 10$ cm constants, which allowed us to evaluate the effect of the void fraction.

Figure 3b presents the transmitted acoustic pressure of the acoustic coatings for varying diameters, considering frequency-dependent and independent complex Young's moduli. It is observed that there is a significant difference between the monopole resonance frequency, the amplitude, and the bandwidth for the two cases, i.e., with (solid lines) and without (dashed lines) frequency-dependent Young's modulus of the PU matrix. The sound attenuation is

Table 2 Monopole resonance for cylinders with different diameters for a polyurethane matrix with and without frequency-dependent Young's modulus and their differences

d/*t*	Void fraction	Monopole resonance (Hz)		Percentage error (%)
		Freq. dependent	Freq. independent	
0.1	0.008	–	2250	–
0.2	0.031	2630	1690	35.7
0.3	0.070	2350	1550	34.0
0.4	0.126	2290	1610	29.7
0.5	0.196	2510	1950	22.3
0.6	0.283	3010	2170	27.9

increased both in amplitude and bandwidth for an increased diameter. This broadband attenuation is attributed to the strong coupling of the voids that correspond to higher filling fractions. However, the sound attenuation is lower for low diameters due to the reduced coupling between voids. This behavior is observed in both cases. We have listed the deviations of the monopole resonance for the frequency-dependent and independent modulus in Table 2.

3.2 Comparison of the performances of different PU matrices

3.2.1 Optimized acoustic coating PU80 with voids

Figure 4a illustrates the geometrical layout of the optimal design that resulted from the developed optimization framework. This design was selected by running the optimization algorithm iteratively and selecting the best option among the solutions as GA does not guarantee the global optimal. The solutions from the iterations converged to similar geometries as shown in Fig. 4a with slight variations in the positioning of the voids. However, the variations in the value of the objective function among these solutions were negligible. Therefore, external factors such as ease of manufacturing and cost can be considered in selecting a suitable solution.

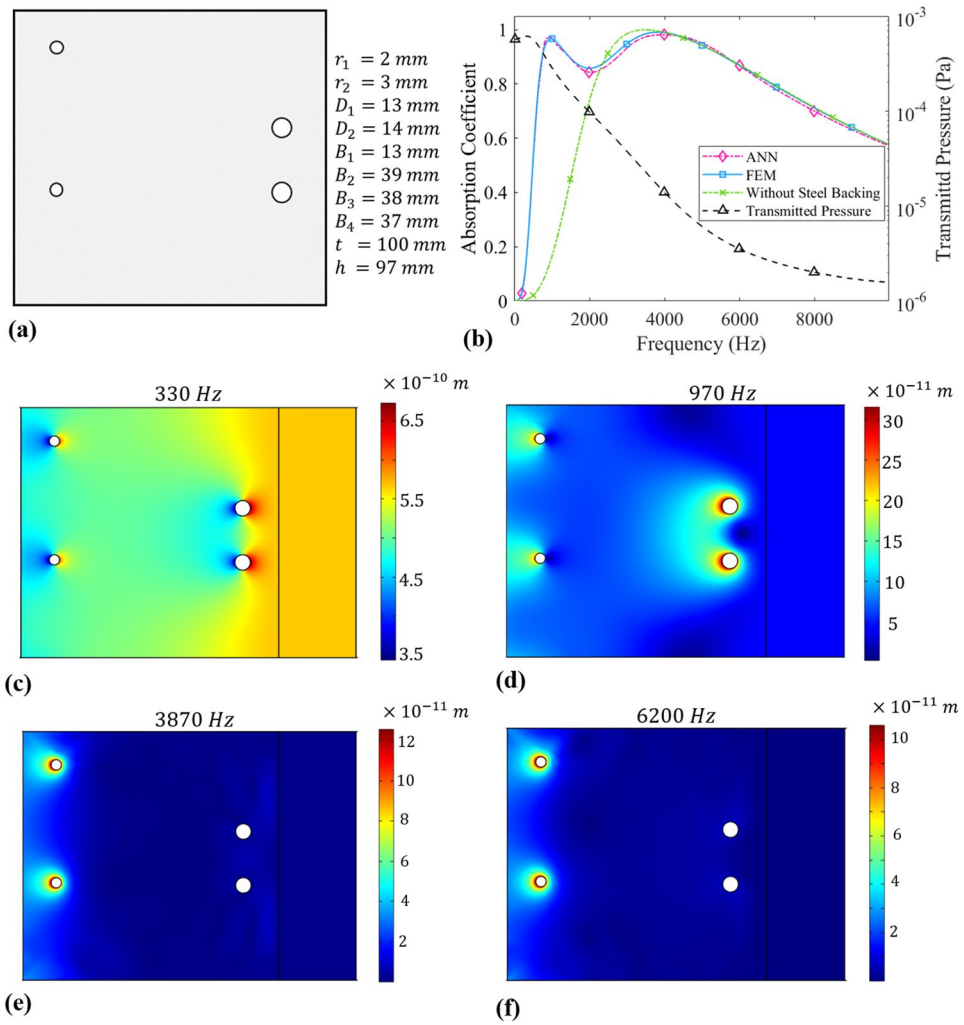

Fig. 4 **a** Geometry of the optimized unit cell with PU80 as the matrix material. **b** Broadband sound attenuation of the optimized unit cell of PU80 with embedded voids and steel backing. Deformation maps at **c** 330 Hz, **d** 970 Hz, **e** 3870 Hz, and **f** 6200 Hz

Moreover, it was observed during the iterative evaluation that the optimal thickness always resided in the upper bound of the acceptable range, i.e., 100 mm. This is because having the largest allowed thickness enables attenuation of acoustic waves with a wider range of wavelengths. Thus, the number of dimensions of the problem can be reduced by fixing the values of these parameters. This enhances the efficiency and the speed of the algorithm as the complexity of the problem can be reduced.

Figure 4b shows the absorption coefficient and the transmitted pressure of the optimized acoustic coating with embedded voids in PU80. The absorption coefficient of the acoustic coating with and without the steel backing is further compared. It is observed that the acoustic coating attached to the steel backing exhibits better broad-band absorption characteristics in the low-frequency range. It consists of two peaks at 970 Hz and 3830 Hz with absorption coefficients of 0.96 and 0.99, respectively. The first peak emerges as a result of the presence of the steel backing at 970 Hz and is attributed to the scattering of the acoustic wave reflected from the steel backing by the layers of the voids. Also, the highest transmission occurs at 330 Hz, and its deflection is presented as a deformation map in Fig. 4c. This high transmission corresponds to the high deflection of the steel plate with a magnitude higher than the deflections at other frequencies. Figure 4d presents the deformation of the second layer of voids that interferes with the reflected wave from the steel backing and displays a radial motion as a result of high sound absorption, this finding is consistent with the previous work (Meng et al. 2012b). From Fig. 4e and f, the first layer of voids that interferes with the incident wave exhibits a radial motion that corresponds to high absorption. This is further confirmed by Fig. 4b that the behavior of acoustic coating with embedded voids in the high-frequency range, i.e., greater than 4000 Hz is independent of the backing.

3.2.2 Optimized acoustic coating PU65 with voids

The optimized geometry of the cylindrical voids in PU65 and its performance is shown in Fig. 5, which is rather similar to the PU80 case. As seen in Fig. S4a, the Young's modulus of PU65 is close to PU80 and from S4b, where

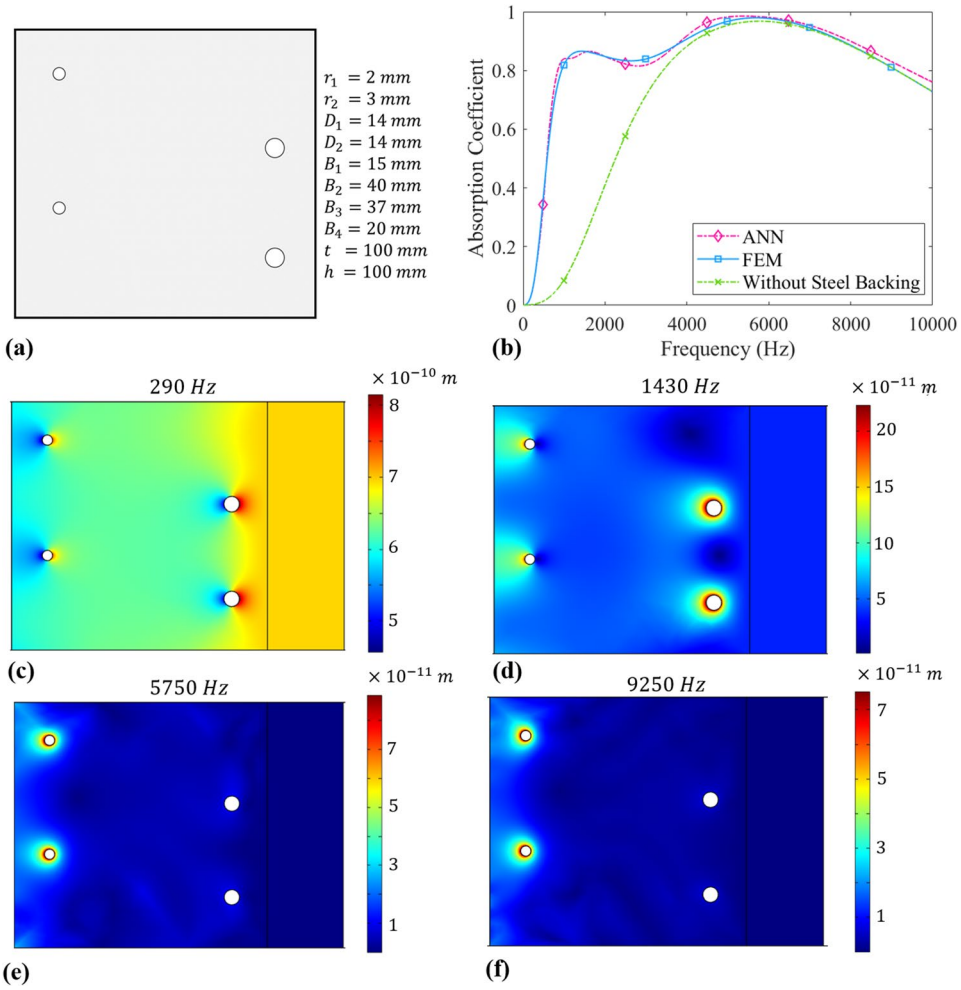

Fig. 5 Geometry of the optimized voids in PU65 (**a**) and absorption coefficient (**b**). Deformation maps of the optimized voids in PU65 at **c** 290 Hz, **d** 1430 Hz, **e** 5750 Hz, and **f** 9250 Hz

both PU65 and PU80 showed low-frequency attenuation with a void of the same diameter. In Fig. 5b the absorption coefficient consists of two peaks at 1430 Hz and 5750 Hz with coefficients of 0.86 and 0.98, respectively. Furthermore, the displacement maps of PU65 at different frequencies are shown in Fig. 5c–f, where PU65 behavior is observed to be similar to that of the PU80.

3.2.3 Optimized acoustic coating PU90 with voids

Figure 6 presents the optimized geometry of the voids in PU90 and its acoustic characteristics. Contrary to PU65 and PU80, the optimal parameters resulted in two layers of voids with larger diameters. PU96 has higher Young's modulus compared to PU65 and PU80. As shown in Section S3.2 an increase in the modulus results in an increase in the speed of sound and therefore, shifts the absorption peaks to higher frequencies. However, as explained in Section S3.3, voids with increased diameters can be used to shift the peak to low frequencies to achieve low-frequency attenuation.

The absorption coefficient of the acoustic coating based on PU90 consists of two peaks at 2130 Hz and 7210 Hz with coefficients of 0.78 and 0.99, respectively. Compared to PU65 and PU80, this corresponds to lower low-frequency sound attenuation. Furthermore, the displacement maps of the unit cell are presented in Fig. 6c–f at different frequencies. The highest deflection of the steel plate occurs at 130 Hz as shown in Fig. 6c and this frequency corresponds to the highest transmission. The first peak at 2130 Hz corresponds to the Fabry–Pérot resonance, and the regions between the voids of minimum displacement, i.e., between the two voids in the right layer correspond(s) to the destructive interference of the sound waves reflected by the steel backing and the voids. At high frequencies, the minimum displacement regions can be seen between the two voids in the left layer that occur mainly due to the interference of the incident wave and sound waves scattered by the four voids. Further, unlike in PU65 and PU80, the effect of the steel backing can be seen throughout the frequency range as shown in Fig. 6.

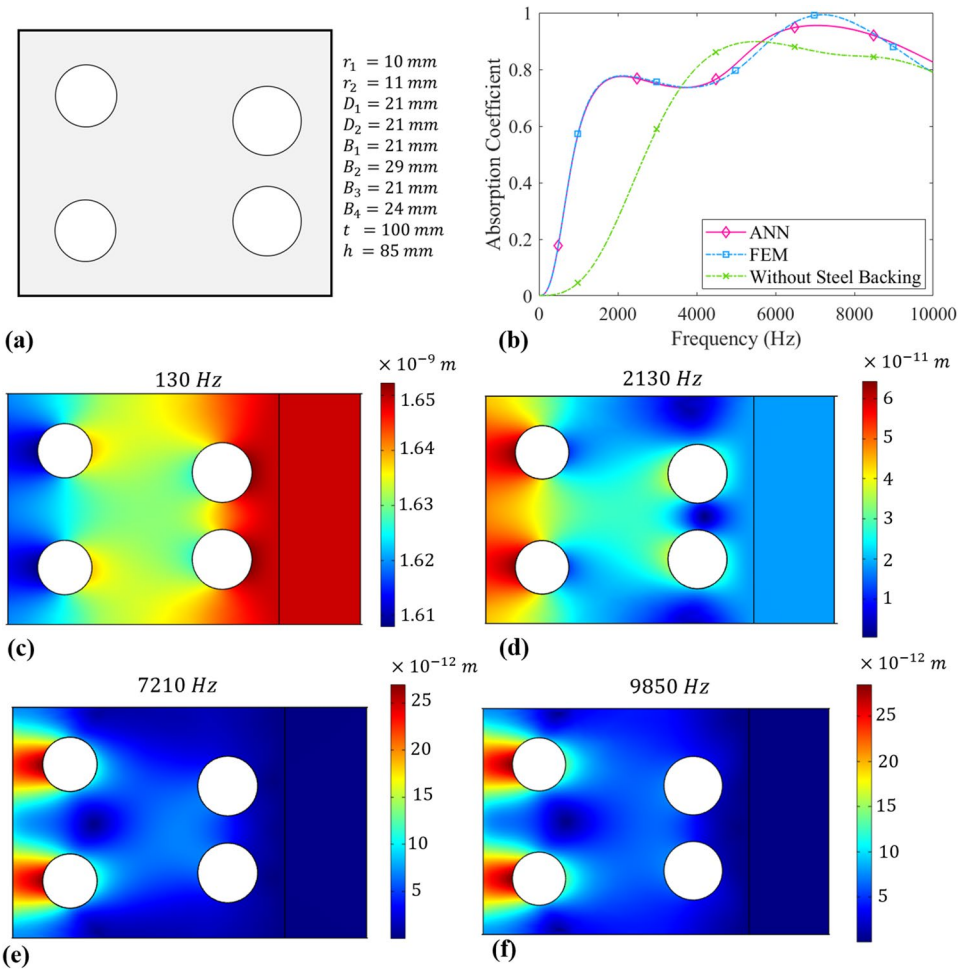

Fig. 6 Geometry of the optimized voids in PU90 (**a**) and absorption coefficient (**b**). Deformation maps of the optimized voids in PU90 at **c** 130 Hz, **d** 2130 Hz, **e** 7210 Hz, and **f** 9850 Hz

4 Summary and Conclusion

We developed an inverse design framework by coupling ML and GA with FEM to develop acoustic coatings comprising cylindrical voids in polyurethane matrix. A FEM-based physical model was used to simulate the realistic acoustic characteristics of the acoustic coatings with embedded voids by accounting for the temperature and frequency dependent Young's modulus of polyurethanes.

In the inverse design, a neural network was incorporated into GA to determine the optimal geometric parameters with maximum broadband sound attenuation at low frequencies. The outcomes of this work demonstrate the developed framework delivers an accelerated inverse design of viscoelastic materials with targeted acoustic performance.

Based on the findings of the present study, we made the following conclusions:

- Acoustic characteristics of coatings with embedded voids depend on multiple factors, including intrinsic material properties of the polymer matrix (specifically frequency-dependent viscoelastic modulus) as well as size and parameters associated with the geometrical layout of the resonant cylindrical voids. Furthermore, it was observed that temperature and frequency-dependency of the moduli of the polymer matrix needs to be considered to obtain accurate and realistic results for the practical application purposes.
- A significant, broadband, low-frequency attenuation was achieved by optimally configuring the layers of cylindrical voids and exploiting attenuation mechanisms, including Fabry–Pérot resonance and Bragg scattering of the layers of voids.
- An optimization algorithm was used for efficient exploration of the design space, which enables accelerated development of acoustic coatings with targeted performance. This provides a tool to overcome conventional time and cost-intensive ad hoc trial-and-error forward design approaches.
- Coupling of ML with the optimization algorithm further accelerates the exploration of the high dimensional design space. The developed DNN exhibited significantly increased speed (by a factor of 4.5×10^3) in predicting the absorption coefficient compared to the FEM.

Although the primary aim of the surrogate ML model in this research is to significantly reduce the prediction time, black box machine leaning models can suffer from issues of interpretability (Angione et al. 2022). To address this issue, we have conducted an extensive parametric study (presented in the supplementary information) and explored the effects of variables to identify the physical mechanisms of sound attenuation. Furthermore, the acoustic characteristics of the coating can be evaluated by different sources of information such as numerical models, analytical models, and experimental data. It is advantageous to leverage these multiple sources of information to accelerate the optimization process. Thus, the current study can be further extended to a multifidelity framework. Another promising direction for future work is to inspect the effect of pressure to assess the performance of coatings under operational conditions. Therefore, the effect of hydrostatic pressure (i.e., operation depth) needs to be incorporated into the design tool.

The significant role of frequency-dependent viscoelastic moduli of the polyurethane matrix on the acoustic performance of these coatings underpins the critical need for establishment of the linkages between polyurethane chemistry (molecular scale) and bulk morphology (mesoscopic scale) to that of the macroscopic viscoelastic behavior (Hajizadeh et al. 2018). These could be achieved through integrating the molecular dynamic simulations (Hajizadeh et al. 2014a, b, 2015; Prathumrat et al. 2021) and self-consistent field theory (Paradiso et al. 2016) calculations into the continuum models in a unified multiscale framework.

Supplementary Information The online version contains supplementary material available at https://doi.org/10.1007/s00158-022-03322-w.

Acknowledgements This research is supported by the Commonwealth of Australia as represented by the Defence Science and Technology Group of the Department of Defence. We acknowledge Melbourne Research Cloud at Faculty of Engineering and Information Technology, The University of Melbourne for providing us the computing facility.

Funding Open Access funding enabled and organized by CAUL and its Member Institutions.

Declarations

Conflict of interest On behalf of all authors, the corresponding author states that there is no conflict of interest.

Replication of results All data that support the findings of this study are included within the article (and supplementary files).

References

Ahmed WW, Farhat M, Zhang X, Wu Y (2021) Deterministic and probabilistic deep learning models for inverse design of broadband acoustic cloak. Phys Rev Res 3:013142

Angione C, Silverman E, Yaneske E (2022) Using machine learning as a surrogate model for agent-based simulations. PLoS ONE 17(2):1–24. https://doi.org/10.1371/journal.pone.0263150

Bacigalupo A, Gnecco G, Lepidi M, Gambarotta L (2020) Machine-learning techniques for the optimal design of acoustic metamaterials. J Optim Theory Appl 187(3):630–653

Bianco MJ, Gerstoft P, Traer J, Ozanich E, Roch MA, Gannot S, Deledalle C-A (2019) Machine learning in acoustics: theory and applications. J Acoust Soc Am 146(5):3590–3628. https://doi.org/10.1121/1.5133944

Cai C, Hung KC, Khan MS (2006) Simulation-based analysis of acoustic absorbent lining subject to normal plane wave incidence. J Sound Vib 291(3):656–680

Calvo DC, Thangawng AL, Layman CN, Casalini R, Othman SF (2015) Underwater sound transmission through arrays of disk cavities in a soft elastic medium. J Acoust Soc Am 138(4):2537–2547

Chang Y-C, Yeh L-J, Chiu M-C (2005) Optimization of double-layer absorbers on constrained sound absorption system by using genetic algorithm. Int J Numer Methods Eng 62(3):317–333

Ciaburro G, Iannace G, Ali M, Alabdulkarem A, Nuhait A (2021) An artificial neural network approach to modelling absorbent asphalts acoustic properties. J King Saud Univ Eng Sci 33(4):213–220

Ciaburro G, Iannace G, Passaro J, Bifulco A, Marano AD, Guida M, Marulo F, Branda F (2020) Artificial neural network-based models for predicting the sound absorption coefficient of electrospun poly(vinyl pyrrolidone)/silica composite. Appl Acoust 169:107472

Donda K, Zhu Y, Merkel A, Fan S-W, Cao L, Wan S, Assouar B (2021) Ultrathin acoustic absorbing metasurface based on deep learning approach. Smart Mater Struct 30(8):085003

Fu Y, Kabir II, Yeoh GH, Peng Z (2021) A review on polymer-based materials for underwater sound absorption. Polym Test 96:107115

Gao R, Zhang Y, Kennedy D (2019) Topology optimization of sound absorbing layer for the mid-frequency vibration of vibro-acoustic systems. Struct Multidisc Optim 59(5):1733–1746. https://doi.org/10.1007/s00158-018-2156-3

Gurbuz C, Kronowetter F, Dietz C, Eser M, Schmid J, Marburg S (2021) Generative adversarial networks for the design of acoustic metamaterials. J Acoust Soc Am 149(2):1162–1174. https://doi.org/10.1121/10.0003501

Hajizadeh E, Todd BD, Daivis PJ (2014a) Nonequilibrium molecular dynamics simulation of dendrimers and hyperbranched polymer melts undergoing planar elongational flow. J Rheol 58(2):281–305

Hajizadeh E, Todd BD, Daivis PJ (2014b) Shear rheology and structural properties of chemically identical dendrimer-linear polymer blends through molecular dynamics simulations. J Chem Phys 141(19):194905

Hajizadeh E, Todd BD, Daivis PJ (2015) A molecular dynamics investigation of the planar elongational rheology of chemically identical dendrimer-linear polymer blends. J Chem Phys 142(17):174911

Hajizadeh E, Yu S, Wang S, Larson RG (2018) A novel hybrid population balance—Brownian dynamics method for simulating the dynamics of polymer-bridged colloidal latex particle suspensions. J Rheol 62(1):235–247

Iannace G, Ciaburro G, Trematerra A (2020) Modelling sound absorption properties of broom fibers using artificial neural networks. Appl Acoust 163:107239

Ivansson SM (2008) Numerical design of Alberich anechoic coatings with superellipsoidal cavities of mixed sizes. J Acoust Soc Am 124(4):1974–1984

Ivansson SM (2012) Anechoic coatings obtained from two- and three-dimensional monopole resonance diffraction gratings. J Acoust Soc Am 131(4):2622–2637

Jayakumari VG, Shamsudeen RK, Ramesh R, Mukundan T (2011) Modeling and validation of polyurethane based passive underwater acoustic absorber. J Acoust Soc Am 130(2):724–730

Jayakumari VG, Shamsudeen RK, Rajeswari R, Mukundan T (2019) Viscoelastic and acoustic characterization of polyurethane-based acoustic absorber panels for underwater applications. J Appl Polym Sci 136(10):47165

Jeon JH, Yang SS, Kang YJ (2020) Estimation of sound absorption coefficient of layered fibrous material using artificial neural networks. Appl Acoust 169:107476

Katoch S, Chauhan SS, Kumar V (2021) A review on genetic algorithm: past, present, and future. Multimed Tools Appl 80(5):8091–8126

Kingma DP, Ba J (2015) Adam: a method for stochastic optimization. In: Bengio Y, LeCun Y (eds) 3rd international conference on learning representations, ICLR 2015, San Diego, May 7-9, 2015, conference track proceedings

Leroy V, Strybulevych A, Lanoy M, Lemoult F, Tourin A, Page JH (2015) Superabsorption of acoustic waves with bubble metascreens. Phys Rev B 91:020301

Li J, Li S (2018) Topology optimization of anechoic coating for maximizing sound absorption. J Vib Control 24(11):2369–2385

Liu Z, Zhang X, Mao Y, Zhu YY, Yang Z, Chan CT, Sheng P (2000) Locally resonant sonic materials. Science 289(5485):1734–1736. https://doi.org/10.1126/science.289.5485.1734

Meng H, Wen J, Zhao H, Wen X (2012a) Optimization of locally resonant acoustic metamaterials on underwater sound absorption characteristics. J Sound Vib 331(20):4406–4416

Meng H, Wen J, Zhao H, Lv L, Wen X (2012b) Analysis of absorption performances of anechoic layers with steel plate backing. J Acoust Soc Am 132(1):69–75

Meyer E, Brendel K, Tamm K (1958) Pulsation oscillations of cavities in rubber. J Acoust Soc Am 30:1116–1124

Montavon G, Samek W, Müller K-R (2018) Methods for interpreting and understanding deep neural networks. Digit Signal Process 73:1–15. https://doi.org/10.1016/j.dsp.2017.10.011

Panigrahi SN, Jog CS, Munjal ML (2008) Multi-focus design of underwater noise control linings based on finite element analysis. Appl Acoust 69(12):1141–1153

Paradiso SP, Delaney KT, Fredrickson GH (2016) Swarm intelligence platform for multiblock polymer inverse formulation design. ACS Macro Lett 5(8):972–976

Prathumrat P, Sbarski I, Hajizadeh E, Nikzad M (2021) A comparative study of force fields for predicting shape memory properties of liquid crystalline elastomers using molecular dynamic simulations. J Appl Phys 129(15):155101

Romero-García V, Sánchez-Pérez J, García-Raffi LM, Herrero J, Garcia-Nieto Rodriguez S, Blasco X (2009) Hole distribution in phononic crystals: design and optimization. J Acoust Soc Am 125:3774–83

Sharma GS, Skvortsov A, MacGillivray I, Kessissoglou N (2017a) Sound transmission through a periodically voided soft elastic medium submerged in water. Wave Motion 70:101–112

Sharma GS, Skvortsov A, MacGillivray I, Kessissoglou N (2017b) Acoustic performance of gratings of cylindrical voids in a soft elastic medium with a steel backing. J Acoust Soc Am 141(6):4694–4704

Sharma GS, Skvortsov A, MacGillivray I, Kessissoglou N (2019) Sound absorption by rubber coatings with periodic voids and hard inclusions. Appl Acoust 143:200–210

Shi K, Jin G, Liu R, Ye T, Xue Y (2019) Underwater sound absorption performance of acoustic metamaterials with multilayered locally resonant scatterers. Results Phys 12:132–142

Sun X, Jia H, Yang Y, Zhao H, Bi Y, Sun Z, Yang J (2021) Acoustic structure inverse design and optimization using deep learning. arXiv preprint arXiv:2102.02063

Wang Y, Zhao H, Yang H, Zhong J, Yu D, Wen J (2021) Inverse design of structured materials for broadband sound absorption. J Phys D 54(26):265301. https://doi.org/10.1088/1361-6463/abf373

Wen J, Zhao H, Lv L, Yuan B, Wang G, Wen X (2011) Effects of locally resonant modes on underwater sound absorption in viscoelastic materials. J Acoust Soc Am 130(3):1201–1208. https://doi.org/10.1121/1.3621074

Wu R-T, Liu T-W, Jahanshahi MR, Semperlotti F (2021) Design of one-dimensional acoustic metamaterials using machine learning and cell concatenation. Struct Multidisc Optim 63(5):2399–2423. https://doi.org/10.1007/s00158-020-02819-6

Wu R-T, Jokar M, Jahanshahi MR, Semperlotti F (2022) A physics-constrained deep learning based approach for acoustic inverse scattering problems. Mech Syst Signal Process 164:108190. https://doi.org/10.1016/j.ymssp.2021.108190

Yu Y, Tong L, Zhao G (2020) Layout optimization of viscoelastic damping for noise control of mid-frequency vibro-acoustic systems. Struct Multidisc Optim 62(2):667–684. https://doi.org/10.1007/s00158-020-02524-4

Yuan B, Chen Y, Tan B, Li B (2019) Statistical optimization of underwater lower-frequency sound insulation for locally resonant sonic material using genetic algorithm. Arch Acoust 44:365–374

Zhao D, Zhao H, Yang H, Wen J (2018) Optimization and mechanism of acoustic absorption of Alberich coatings on a steel plate in water. Appl Acoust 140:183–187

Zheng B, Yang J, Liang B, Cheng J (2020) Inverse design of acoustic metamaterials based on machine learning using a Gauss-Bayesian model. J Appl Phys 128(13):134902. https://doi.org/10.1063/5.0012392

Zhong J, Zhao H, Yang H, Wang Y, Yin J, Wen J (2019) Theoretical requirements and inverse design for broadband perfect absorption of low-frequency waterborne sound by ultrathin metasurface. Sci Rep 9(1):1181. https://doi.org/10.1038/s41598-018-37510-w